Spatial Reconstruction of Rain Fields From Wireless Telecommunication Networks—Scenario-Dependent Analysis of IDW-Based Algorithms

Adam Eshel, Jonatan Ostrometzky, *Member, IEEE*, Shani Gat, Pinhas Alpert, Hagit Messer, *Fellow, IEEE*

***Abstract*— In the last decade, commercial microwave links (CMLs) have been treated as opportunistic near-ground rain sensors, and successfully used for the retrieval of 2-D near-ground rain fields in several countries. In spite of the path integration of a CML, most studies represent the rainfall measured by a CML as a single virtual rain gauge (VRG) in the center of the path. Here, we study the performance of spatial reconstruction of rain fields by an inverse distance weighting (IDW) spatial interpolation method. We compare the case where each CML is represented by a single VRG with the case where it is represented by several VRGs along its path. A synthetic rain field was produced, simplified to a single rain cell, and sampled by a synthetic CML network that was built according to statistics of actual CMLs. A Monte Carlo simulation study yielded a quantitative and specific set of metrics showing that the rain-retrieval results are scenario-dependent and can be used to design a rain-retrieval system. In particular, we show that if the rain-cell dimensions are in the order of the average length of the CMLs, using several VRG with the iterative algorithm can significantly improve the retrieval performance, whereas the performance gain is small otherwise.**

***Index Terms*— Commercial microwave links (CMLs), rainfall monitoring, spatial interpolation.**

I. Introduction

UNDERSTANDING the rain-field spatiotemporal behavior has drawn considerable attention of various research fields from physically based hydrometeorological forecasting models to processing and analysis of observations. Utilizing the cellular communication microwave-based backhaul infrastructure for rainfall monitoring was introduced over a decade ago [1], [2]. Nowadays, the use of commercial microwave links (CMLs) to regularly collect signal level measurements for rain monitoring has been well studied, appropriate algorithms were introduced (e.g., [3]–[6]), and the technology is almost ready for applicable uses, e.g., national/international meteorological/hydrological services [7] as well as private weather forecasting and nowcasting providers. As a consequence of their nature, CMLs provide a near-ground-level representation of rain as a line projection and not as a point sample, traditionally undertaken by rain gauges (RGs). Nonetheless, most 2-D rain mapping methods treat each CML as a single virtual RG (VRG), which is commonly positioned in the center of the CML path [5], [8]. Representing a CML by a point measurement in space brings both challenges and opportunities when it comes to 2-D rain field reconstruction. On the one hand, the length allows a larger coverage, which increases the potential detection probability. On the other hand, when rain distribution along the CML is not uniform, an inherent error is added. The performance of the rainfall 2-D estimations is highly dependent on the characteristics of the CML network. The latter varies for different population densities, in spatial density (number of links per km^2) and average length; the more (less) urbanized an area, the higher (lower) the CMLs' density and the smaller (larger) their mean length [9].

Most studies employing CMLs for rain mapping implement well-established methodologies of field reconstruction (e.g., [10]–[12]), such as inverse distance weighting (IDW) interpolation [13], [14], or given sufficient knowledge regarding rain statistics, the Kriging approach [15], [16]. Furthermore, it was suggested to use the dynamic information of rain, derived from multiple snapshots, for the interpolation of the rain field [17]. Relations between CMLs and RGs or other weather-monitoring instruments were inspected in previous studies [18]–[20], and it was suggested to treat the CML attenuation measurements as line-projection samples [21], [22]. Also, utilizing tomography [23], [24], implementing sparse modeling with compressed sensing tools [25], [26], and using object tracking techniques [27] have been studied. In addition, it has been suggested to set multiple VRGs by dividing each CML into nonoverlapping subsections [28]. The aforementioned study also proposed using neighboring links in an IDW-based iterative algorithm (hereafter GMZ after the authors' initials) to adjust the values of the different VRGs, when used for 2-D rain mapping. While long-term studies conducted in the Netherlands demonstrated that representing a link by a single VRG is sufficient for reliable 2-D rain reconstruction [10], the potential benefit, if any, of considering more VRGs per link has not yet been investigated.

Manuscript received April 10, 2019; revised July 14, 2019; accepted August 10, 2019. This work was supported by the German Research Foundation (DFG) through the project "Integrating Microwave Link Data for Analysis of Precipitation in Complex Terrain: Theoretical Aspects and Hydrometeorological Applications (IMAP)." *(Corresponding author: Adam Eshel.)*

A. Eshel and P. Alpert are with the Department of Geophysics, Tel Aviv University, Tel Aviv-Yafo 6997801, Israel (e-mail: adameshel@mail.tau.ac.il).

J. Ostrometzky is with the Department of Electrical Engineering, Columbia University in the City of New York, New York, NY 10027 USA.

S. Gat and H. Messer are with the School of Electrical Engineering, Tel Aviv University, Tel Aviv-Yafo 6997801, Israel.

Color versions of one or more of the figures in this letter are available online at http://ieeexplore.ieee.org.

Digital Object Identifier 10.1109/LGRS.2019.2935348

A given rain intensity 2-D field $R(x, y)$ (in mm h^{-1}), attenuates microwave signals between a transmitter and a receiver approximated by *Power-Law* relations [29]

$$A = a \int_0^L R(l)^b \, \mathrm{d}l \quad \text{(dB)} \tag{1}$$

where L is the length of the CML and a and b are empirical parameters [30]. The discrete equivalent of (1) when a CML is divided to i segments can be written as

$$A = a \sum_i R_i^b \, \Delta l \quad \text{(dB)} \tag{2}$$

where the values of R_i can naturally differ from one another. Equation (2) is based on the assumption that Δl is such that the rain over the segment is approximately constant, and is given by R_i. Thus, in the case of a single VRG in the center of a CML, the approximation $R(l) = R_0$ implies that Δl is the full CML length, and therefore, yields

$$A \approx a R_0^b L \quad \text{(dB)}. \tag{3}$$

This case can also be written as (2) where $R_i = R_0$ for all i in order to exploit the length of the link

$$A = a R_0^b \sum_i \Delta l \quad \text{(dB)}. \tag{4}$$

Alternatively, GMZ allows R_i along a single CML to differ, and therefore, suggests a better approximation of (2).

When attempting to reconstruct rain fields, three fundamental aspects must be addressed upon which the performance of the rain field reconstruction depends: 1) the given CML network; 2) the nature of the rain field; and 3) the desired reconstruction field scale. The aforementioned aspects properties dictate the quality of the CML-based rain-field reconstruction accuracy.

In this letter, we study the potential improvement in performance, if any, of 2-D rain field reconstruction using spatial interpolation by using more than a single VRG to represent a link. To be able to present quantitative results, the ground truth must be available. Therefore, we simulated a rain field by a 2-D Gaussian-shape rain cell, where the intensity of the rain and its spatial coverage can be controlled by a finite set of parameters. It is common to use the Gaussian shape for spatial representation in stochastic rainfall modeling, although there are other shapes that better fit different rainfall patterns [31]. Since a real rain cell can be reasonably reconstructed by a combination of a finite number of Gaussian shapes, a single Gaussian constitutes a simplified case, so that we could isolate the spatial variability challenges. A synthetic CML network had been simulated as well, following the statistics of operational networks [9]. Monte Carlo simulations, in which a randomly chosen location of an increase in size "rain cell" was generated, were applied. Regarding the characteristics of the sampling CML network, we showed a significant reduction of error can be achieved in reconstructing rain fields, for a confined range of rain cell sizes, when multiple VRGs represent the CML and GMZ is utilized.

The rest of this letter is organized as follows: In Section II, we describe the compared interpolation methodologies, present the steps taken in structuring the synthetic experiment, and explain the performance grading method. In Section III, we analyze the results of the Monte Carlo simulations performed. Finally, Section IV concludes this letter.

II. Methodology

A. Methodologies Compared

The IDW weighting function (Shepard's method) describing the weight of the ith VRG, by which the spatial interpolation is done, is given as

$$w_i = \frac{\left(1 - \frac{d_i}{D}\right)^2}{\left(\frac{d_i}{D}\right)^2}, \quad \text{if } \frac{d_i}{D} < 1 \tag{5}$$

where d_i is the distance between VRG_i and a target grid point, and D is the distance beyond which VRG_i ceases to effect d_i, i.e., radius of influence (here 10 km). The IDW based interpolation methodologies compared in this study were:

1) IDW1, IDW3, and IDW9; for M CMLs, each is represented by one, three, and nine VRGs resulting in M, $3M$, and $9M$ VRGs, respectively. The value measured by each VRG is the averaged rain along the link R_0 and is the same for all VRGs. Rain field reconstruction is done by IDW with all VRGs;
2) GMZ3, GMZ9, and GMZ13 are 3, 9, and 13 VRGs per CML, respectively. After the convergence of GMZ, the VRGs can have different values. IDW is subsequently executed utilizing all VRGs.

Parameters of GMZ algorithm used here were: 1) predefined root mean square differences convergence tolerance threshold (10^{-4} mm h^{-1}), between VRGs values in a given iteration and the previous to it and 2) a limitation of the maximum number of iterations to 28.

B. Synthetic CML Network and Rainfall Ground Truth Generation

Strong relations between the CML averaged length (hereafter L_m) and the spatial density of the network have been shown in a recent study [9], suggesting that long (short) L_m is associated with the low (high) spatial density of CMLs. Based on the existing properties of CMLs in suburban areas in Israel, a synthetic net of links was generated with $L_m = 2.5$ km and a spatial density of 0.53 km^{-2} as follows: First, the locations of K centers of links were randomly selected within an area of approx. 16×16 km^2, and an additive independent and identically distributed (iid) Gaussian samples, $n_x^i \sim N(0, 200\ \mathrm{m})$, $n_y^i \sim N(0, 200\ \mathrm{m})$; $i \in \{1, 2, \cdots, K\}$, were generated and used as an additive Gaussian noise to the locations. Thus, each center i is located at: $\{x_i + n_x^i, y_i + n_y^i\}$. Then, the length of each of the CML was randomly generated using an exponential distribution[1] with L_m as the scale parameter. The angular orientations of each of the CMLs, α_i, were uniformly generated: $\alpha_i \sim U(0, \pi)$. The frequencies and polarization were assigned

[1]Please note that due to practical reasons, only lengths between 1 and 10 km were considered, making the CMLs' lengths a truncated exponentially distributed sample-set.

according to their appearances in that specific region (one-third of the CMLs were assigned horizontal polarization, and two-thirds to vertical), considering practical use (longer links were assigned with lower frequencies).

A dedicated *Rain Simulator* converting continuous spatial simplified rain cells into path microwave attenuation was built. In an attempt to isolate the effect of the intermittency of the rain as much as possible, a single Gaussian-shape was used to represent the 2-D spatial rain field as

$$R(\bar{x}_1, , \bar{x}_k) = A_r \exp\left(-\frac{1}{2}(\bar{x}-\bar{\mu})^T \Sigma^{-1}(\bar{x}-\bar{\mu})\right) \quad (6)$$

where $\bar{x}$ is a vector containing the spatial coordinates (x, y); $\bar{\mu}$ is the location vector (μ_X, μ_Y) of the center of the Gaussian; A_r (given in mm h^{-1} or simply in depth units, e.g., millimeter) is the amplitude, i.e., rain intensity in the center of the Gaussian; $\sum$ is the covariance matrix diagonal with $\sigma = \sigma_X = \sigma_Y$ for simplicity. Monte Carlo simulations were performed as follows: μ_X and μ_Y were randomly chosen N times for each increasing σ ($N = 10$ except when noted otherwise). The lower and higher 15% of each of the 2-D plane dimensions were restricted for μ_X and μ_Y in order to avoid considerable truncation of the Gaussian shapes resulting from (6).

The values of σ correspond with the radius of the effective part of the rain cell. Therefore, in order to characterize its size, the diameter (D_{rc}) can be comparable to $(\bar{\mu}+\sigma)-(\bar{\mu}-\sigma)$, i.e., to 2σ. The values of D_{rc} begin with 400 m, inferring on a very small cell, and gradually increase up to 20 km, a spatial pattern closer to uniform in the given domain. Each simulated rainfall was, in turn, gridded to the resolution of approx. 300×300 m^2 and was used as ground truth for the assessment of the performance analysis of the reconstructing algorithms.

During the operation of the *Rain Simulator*, the value of the attenuation induced upon the ith CML was determined by (1). For the sake of making the simulations closer to reality measurements, these attenuation values undergo quantization (0.1 dB) after having assigned additive Gaussian noise to $n \sim N(0, (0.1^2/12))$ [28]. When working with actual measurements, one must account to "other than rain" attenuation factors by applying methods of baseline determination. Here, the "other than rain" factors did not exist, reducing a major factor of uncertainty [32]–[34]. While for our focused research question these uncertainties were not addressed, in future studies we plan to include them. Once the *Rain Simulator* induced the attenuation upon each of the links in the given network, the different rain reconstruction algorithms were applied to retrieve the simulated rain field.

After the rain fields from the different algorithms were reconstructed, the root mean square error (RMSE) and the correlation coefficient (r) of each one with its ground truth were calculated. The scores of RMSE for each D_{rc} were averaged over the N Monte Carlo runs as

$$\mathrm{RMSE} = \frac{1}{N}\sum_{n=1}^{N}\sqrt{\frac{\sum_{p=1}^{P}(\hat{R}_p - R_p)^2}{P}} \quad (\mathrm{mm}\ h^{-1}) \quad (7)$$

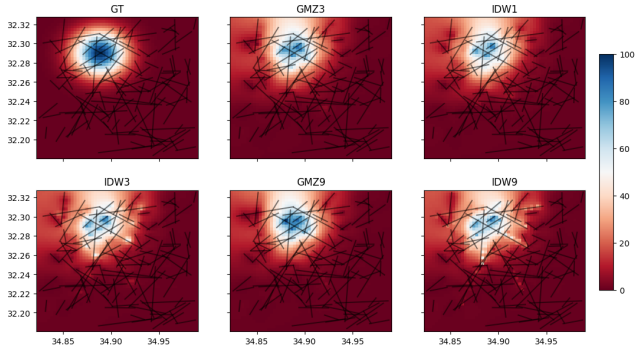

Fig. 1. Example of a simulated Gaussian-shape rain field (D_{rc}=1400 m) and the reconstructed image of the tested algorithms, presented on the synthetic CML network. The rain intensity scale is given in mm h^{-1} and can also refer to as rain depth. The horizontal and vertical axes are the representative latitudes and longitudes of the area from which the CML network characteristics were taken [9].

where P is the number of pixels in a reconstructed grid, and $\hat{R}_p$ and R_p are the estimated and the ground truth rain intensity in pixel p, respectively. For presentation purposes, the score of the aforementioned r was averaged in a similar manner. A rain-intensity-normalized RMSE (RMSE_R) analysis was performed similar to that of RMSE

$$\mathrm{RMSE}_R = \frac{1}{N}\sum_{n=1}^{N}\frac{1}{R_{\mathrm{AVG}}}\sqrt{\frac{\sum_{p=1}^{P}(\hat{R}_p - R_p)^2}{P}} \quad (-) \quad (8)$$

where R_{AVG} is derived from the ground truth for the nth simulation as

$$R_{\mathrm{AVGn}} = \frac{\sum_{p=1}^{P} R_p}{P} \quad (\mathrm{mm}\ h^{-1}). \quad (9)$$

A demonstration of one of the simulated rain fields, the synthetic network and the reconstruction image of all methodologies tested, is shown in Fig. 1.

III. Results

In Fig. 2, the rain field retrieval performances, namely, the RMSE, RMSE_R, and r performance measures, are shown where the maximum rain rate at point (μ_x, μ_y) is $A_r = 100$ mm h^{-1}. All algorithms present poor performance for extremely small rain cell and excellent performance for large rain cells, where the rain over the links is practically constant. This is indicated by reasonable values of r, first obtained for rain cells with $D_{rc} \geq 1000$ m, suggesting a critical size of rain cell which can be detected and/or reconstructed by a given network. Interestingly, a division between the GMZ and noniterative algorithms can be noticed, starting at small rain cells, where a clear hierarchy is formed in a descending order, from GMZ13 to GMZ3. A counter-hierarchy is formed among the three noniterative spatial interpolation cases, where the more VRGs per CML there are, the worse the performance is. Shrinking of the differences between all reconstruction methods occurs in large Gaussians, where all of them perform well. Although one can anticipate this behavior as the CML samples are more alike due to the closer-to-uniform distribution of the rain field.

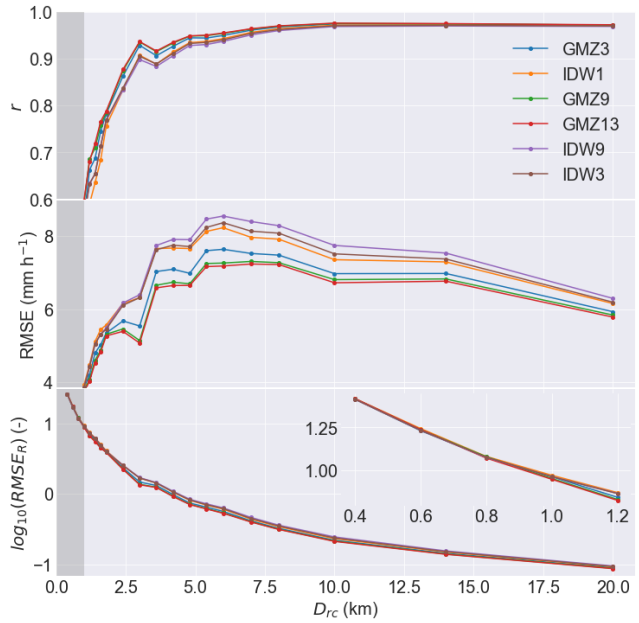

Fig. 2. (Top to bottom) Performance measures: correlation (r), absolute error (RMSE), and relative error (RMSE$_R$) with respect to rain cell diameters. RMSE emphasizes the extent of the performance hierarchy. r and RMSE$_R$ infer on the validity of the reconstruction for the different rain cell sizes. Enlargement of RMSE$_R$ for small rain cells is also presented, in which differences between the tested algorithms are not noticeable. Results were averaged over $N = 10$ Monte Carlo simulations, for all interpolation algorithms. Shaded areas, marked for small rain cells, for which the correlations with the ground truth were poor ($r < 0.6$).

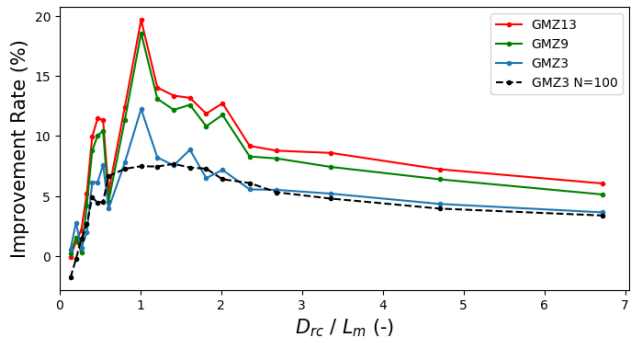

Fig. 3. RMSE improvement rate (in percentage) of GMZ3, GMZ9, and GMZ13 versus IDW1. Results are plotted against the rainfall cell size relative to the spatial properties of the network. A simulation with $N = 100$ and $A_r = 25$ solely for GMZ3, is displayed as well. The smoother line indicates that the strong variations in GMZ9 and GMZ13 are expected to be more moderate with a larger number of simulations. GMZ constantly improves RMSE performance but has negligible additional contribution when more than nine VRGs are used.

The improvement rate of RMSEs when GMZ is utilized over the commonly used IDW1 is displayed in Fig. 3. In addition, a Monte Carlo simulation with $N = 100$ was conducted (only for GMZ3 due to computing resources limitations) with $A_r = 25$, is displayed. The horizontal axis, D_{rc}/L_m, represents the ratio between the size of the rain cell and the average length of the links, which also characterizes the density of the CML network [9]. It is inferred that a substantial diminishing of the estimation error can be achieved in a range of rain cell sizes, most of which are on the order of L_m. Although in larger rain cells the improvement rate declines, according to Fig. 3, worsening of the reconstruction accuracy was not identified. Moreover, as expected, in the simulation in which $N = 100$, $A_r = 25$ is smoother than in the $N = 10$ case, but the improvement rate in RMSE presents resembling values, implying on close to complete independence of actual rain intensities.

IV. Discussion and Conclusion

A comparative study addressing the challenge of spatial interpolation and reconstruction of rain fields was conducted, contrasting the accuracy of estimated 2-D rain maps created from simulated CML attenuation measurements. Our main focus was centered around the amount of VRGs needed to adequately represent a CML by, and in which cases there is an added value applying an iterative algorithm, utilizing neighboring CMLs. By setting more VRGs per link, two important benefits take place: 1) the length of the whole link is better utilized and 2) there is more room for rain intensity variations along the path.

It is noticeable that a substantial part of the rain cell size spectrum, i.e., in large rain cell sizes, the differences between the tested algorithms is rather small. However, for cases in which D_{rc} is in the order of L_m, exploiting an iterative algorithm, rather than IDW1, can improve RMSE by 20% (for GMZ13). After a peak associated with D_{rc}/L_m around 1, toward larger rain cells, the contribution of GMZ is diminished, but so does the slope, inferring on GMZ being slightly preferable even in larger rainfall coverage. This can also be seen as even when D_{rc} is greater than $6L_m$, the potential improvement is around 5%. Notwithstanding, stabilizing of the improvement rate, with the addition of VRGs, can be noticed from Fig. 3. When six VRGs are added from GMZ3 to form the GMZ9 case, the improvement rate is not as significant as the one from IDW1 to GMZ3. Between GMZ9 and GMZ13 the improvement rate is small to negligible. Note, however, that overfitting can potentially take place with a further increasing number of VRGs.

The fact that reconstructions of small D_{rc}s cells are associated with poor correlations alongside low RMSEs, is not surprising. As in these cases, the majority of the pixels (both in the ground truth and in the reconstructions) hold very low values, the relative error is rather high, but the mean absolute error is low. Looking at RMSE$_R$, (Fig. 2) solves this by presenting high values for small cells. However, RMSE$_R$ should still be complementary to RMSE since it might create a misleading effect with real data: dependence on the average rain intensity, which can lead to wrong grading of different types of spatially distributed rainfall patterns. It is possible that the solution for real data, in cases where low rain intensities are of lower interest, is setting a threshold of rain intensity, below which pixels are discarded from the analysis.

It was also found that the division of a CML to more than one VRG with identical measurements devalues the accuracy of the reconstructed rain field when a noniterative IDW is exploited. A possible explanation is that the division of a CML into more evenly spaced VRGs is, de facto, an exploitation of the length dimension, and since deciding that the center of the CML represents the measured rain intensity holds an inherent error, applying that error onto more locations along the CML path should be expected to be more harmful than beneficial.

That alone can explain the poor RMSEs performed by IDW3, and even more poorly by IDW9, when small rain cells are sampled. Since only synthetic data were used in this study, it was highly controllable.

In this letter, we analyzed and compared the performance of spatial reconstruction of rain fields, based on the IDW algorithm for spatial interpolation, where the virtual measurements points were extracted from the CMLs using different methods. We based our analysis on simulated data, as an accurate and controllable data set as a ground truth was required. Indeed, our simulated data were generated based on real-world statistics. However, actual real-world events could have additional characteristics (different numbers of rain cells, rain cells with various rain intensities, different quantization levels, etc.). Thus, future research is required to study the sensitivity of our results to real-world conditions. Moreover, while this study was done for a specific spatial interpolation method, the quantitative improvement of the 2-D reconstruction may also be dependent on it. This is also an issue for a future study.

To conclude, our study suggests that when reconstructing a rain field from measurements taken by a CML network using spatial interpolation methods, a major factor that influences the accuracy is the ratio between the size of a typical rain cell, and the density/average length of the links. If this ratio is much smaller or much larger than one, then representing each link by a single VRG is sufficiently good, and the tradeoff decision between computing time and a potential improvement lies in front of the user. If, however, the ratio is on the order of one, it is possible to improve accuracy significantly by applying GMZ [28] with more than a single VRG per link. Note, however, that while GMZ always performs better than IDW1, setting several VRGs (of identical rain values) per link deteriorates the performance.

ACKNOWLEDGMENT

The authors would like to thank D. Serebrenik for his technical support.

REFERENCES

[1] H. Messer, A. Zinevich, and A. Pinhas, "Environmental monitoring by wireless communication networks," *Science*, vol. 312, no. 5774, p. 713, 2006.

[2] H. Leijnse, R. Uijlenhoet, and J. N. M. Stricker, "Rainfall measurement using radio links from cellular communication networks," *Water Resour. Res.*, vol. 43, p. 3, Mar. 2007.

[3] C. Chwala, F. Keis, and H. Kunstmann, "Real-time data acquisition of commercial microwave link networks for hydrometeorological applications," *Atmos. Meas. Technol.*, vol. 9, no. 3, pp. 991–999, Mar. 2016.

[4] J. Ostrometzky, R. Raich, A. Eshel, and H. Messer, "Calibration of the attenuation-rain rate power-law parameters using measurements from commercial microwave networks," in *Proc. IEEE Int. Conf. Acoust., Speech Signal Process. (ICASSP)*, Shanghai, China, Mar. 2016, pp. 3736–3740.

[5] A. Overeem, H. Leijnse, and R. Uijlenhoet, "Retrieval algorithm for rainfall mapping from microwave links in a cellular communication network," *Atmos. Meas. Tech.*, vol. 9, no. 5, pp. 2425–2444, 2016.

[6] J. Ostrometzky, A. Eshel, P. Alpert, and H. Messer, "Induced bias in attenuation measurements taken from commercial microwave links," in *Proc. IEEE Int. Conf. Acoust., Speech Signal Process. (ICASSP)*, New Orleans, LA, USA, Mar. 2017, pp. 3744–3748.

[7] L. Bao *et al.*, "A brief description on measurement data from an operational microwave network in Gothenburg, Sweden," in *Proc. 15th Int. Conf. Environ. Sci. Technol.*, Rhodes, Greece, vol. 31, 2017, pp. 1–5.

[8] J. C. M. Andersson, P. Berg, J. Hansryd, A. Jacobsson, J. Olsson, and J. Wallin, "Microwave links improve operational rainfall monitoring in Gothenburg, Sweden," in *Proc. CEST*, 2017, pp. 1–4.

[9] L. Gazit and H. Messer, "Advancements in the statistical study, modeling, and simulation of microwave-links in cellular backhaul networks," *Environments*, vol. 5, no. 7, p. 75, 2018.

[10] A. Overeem, H. Leijnse, and R. Uijlenhoet, "Country-wide rainfall maps from cellular communication networks," *Proc. Nat. Acad. Sci. USA*, vol. 110, no. 8, pp. 2741–2745, 2013.

[11] F.-W. Chen and C.-W. Liu, "Estimation of the spatial rainfall distribution using inverse distance weighting (IDW) in the middle of Taiwan," *Paddy Water Environ.*, vol. 10, no. 3, pp. 209–222, 2012.

[12] C. Chwala and H. Kunstmann, "Commercial microwave link networks for rainfall observation: Assessment of the current status and future challenges," *Wiley Interdiscipl. Rev., Water*, vol. 6, no. 2, p. e1337, 2019.

[13] B. Ahrens, "Distance in spatial interpolation of daily rain gauge data," *Hydrol. Earth Syst. Sci. Discuss.*, vol. 2, no. 5, pp. 1893–1922, 2005.

[14] G. Y. Lu and D. W. Wong, "An adaptive inverse-distance weighting spatial interpolation technique," *Comput. Geosci.*, vol. 34, no. 9, pp. 1044–1055, 2008.

[15] N. Cressie, "The origins of Kriging," *Math. Geol.*, vol. 22, no. 3, pp. 239–252, Apr. 1990.

[16] M. L. Stein, *Interpolation of Spatial Data: Some Theory for Kriging*. Berlin, Germany: Springer, 2012.

[17] V. Roy, S. Gishkori, and G. Leus, "Dynamic rainfall monitoring using microwave links," *EURASIP J. Adv. Signal Process.*, vol. 2016, no. 1, pp. 1–17, 2016.

[18] A. Zinevich, H. Messer, and P. Alpert, "Prediction of rainfall intensity measurement errors using commercial microwave communication links," *Atmos. Meas. Technol.*, vol. 3, no. 5, pp. 1385–1402, Oct. 2010.

[19] H. Leijnse, R. Uijlenhoet, and A. Berne, "Errors and uncertainties in microwave link rainfall estimation explored using drop size measurements and high-resolution radar data," *J. Hydrometeorol.*, vol. 11, no. 6, pp. 1330–1344, Dec. 2010.

[20] M. Fencl, J. Rieckermann, P. Sýkora, D. Stránský, and V. Bareš, "Commercial microwave links instead of rain gauges: Fiction or reality?" *Water Sci. Technol.*, vol. 71, no. 1, pp. 31–37, 2015.

[21] O. Sendik, "On the coverage and reconstructability of 2D functions sampled by arbitrary line projections with an application to rain field mapping," M.S. thesis, School Elect. Eng., Tel Aviv Univ., Tel Aviv, Israel, 2013.

[22] H. Messer and O. Sendik, "A new approach to precipitation monitoring: A critical survey of existing technologies and challenges," *IEEE Signal Process. Mag.*, vol. 32, no. 3, pp. 110–122, May 2015.

[23] D. Giuli, A. Toccafondi, G. B. Gentili, and A. Freni, "Tomographic reconstruction of rainfall fields through microwave attenuation measurements," *J. Appl. Meteorol.*, vol. 30, no. 9, pp. 1323–1340, 1991.

[24] D. Giuli, L. Facheris, and S. Tanelli, "Microwave tomographic inversion technique based on stochastic approach for rainfall fields monitoring," *IEEE Trans. Geosci. Remote Sens.*, vol. 37, no. 5, pp. 2536–2555, Sep. 1999.

[25] Y. Liberman and H. Messer, "Accurate reconstruction of rain field maps from Commercial Microwave Networks using sparse field modeling," in *Proc. ICASSP*, May 2014, pp. 6786–6789.

[26] L. Gazit and H. Messer, "Sufficient conditions for reconstructing 2-D rainfall maps," *IEEE Trans. Geosci. Remote Sens.*, vol. 56, no. 11, pp. 6334–6343, Nov. 2018.

[27] Y. Liberman, "Object tracking extensions for accurate recovery of rainfall maps using microwave sensor network," in *Proc. 22nd Eur. Signal Process. Conf. (EUSIPCO)*, Sep. 2014, pp. 1322–1326.

[28] O. Goldshtein, H. Messer, and A. Zinevich, "Rain rate estimation using measurements from commercial telecommunications links," *IEEE Trans. Signal Process.*, vol. 57, no. 4, pp. 1616–1625, Apr. 2009.

[29] *Attenuation Due to Clouds and Fog*, document ITU-R.840, 840-6, 2013.

[30] *Specific Attenuation Model for Rain for Use in Prediction Methods*, document ITU-R.838, 838-3, 1992-1999-2003-2005, 2005.

[31] J. Von Hardenberg, L. Ferraris, and A. Provenzale, "The shape of convective rain cells," *Geophys. Res. Lett.*, vol. 30, no. 24, p. 2280, 2003.

[32] M. Schleiss and A. Berne, "Identification of dry and rainy periods using telecommunication microwave links," *IEEE Geosci. Remote Sens. Lett.*, vol. 7, no. 3, pp. 611–615, Jul. 2010.

[33] M. Schleiss, J. Rieckermann, and A. Berne, "Quantification and modeling of wet-antenna attenuation for commercial microwave links," *IEEE Geosci. Remote Sens. Lett.*, vol. 10, no. 5, pp. 1195–1199, Sep. 2013.

[34] H. Leijnse, R. Uijlenhoet, and J. N. M. Stricker, "Microwave link rainfall estimation: Effects of link length and frequency, temporal sampling, power resolution, and wet antenna attenuation," *Adv. Water Resour.*, vol. 31, pp. 1481–1493, Nov. 2008.